Manuscript submitted to
AIMS' Journals
Volume **X**, Number **0X**, XX **200X**

Website: http://AIMsciences.org

pp. **X–XX**

DISSIPATIVE AND WEAKLY–DISSIPATIVE REGIMES IN NEARLY–INTEGRABLE MAPPINGS

Alessandra Celletti

Dipartimento di Matematica
Università di Roma Tor Vergata
Via della Ricerca Scientifica 1
I-00133 Roma (Italy)

Claude Froeschlé

Observatoire de Nice
B.P. 229
06304 Nice Cedex 4 (France)

Elena Lega

Observatoire de Nice
B.P. 229
06304 Nice Cedex 4 (France)

(Communicated by Aim Sciences)

Abstract. We consider a dissipative standard map–like system, which is governed by two parameters measuring the strength of the dissipation and of the perturbation. In order to investigate the dynamics, we follow a numerical and an analytical approach. The numerical study relies on the frequency analysis and on the computation of the *differential* fast Lyapunov indicators. The analytical approach is based on the computation of a suitable normal form for dissipative systems, which allows to derive an analytic expression of the frequency.
We explore different kinds of attractors (invariant curves, periodic orbits, strange attractors) and their relation with the choice of the perturbing function and of the main frequency of motion (i.e., the frequency of the invariant trajectory of the unperturbed system). In this context we investigate also the occurrence of periodic attractors by looking at the relationship between their periods and the parameters ruling the mapping. Particular attention is devoted to the investigation of the weakly chaotic regime and its transition to the conservative case.

1. **Introduction.** Many physical phenomena can be conveniently described in terms of nearly–integrable weakly dissipative systems. To be concrete, let us quote an example borrowed from Celestial Mechanics. Consider an oblate satellite moving on a Keplerian orbit around a primary body. As far as the satellite is assumed to be a rigid body of triaxial ellipsoidal form, the dynamical system is described by a nearly–integrable Hamiltonian, where the perturbing parameter represents the equatorial oblateness of the satellite. If one releases the rigidity assumption, one must face a dissipative problem, where the dissipation represents the tidal distortion

2000 *Mathematics Subject Classification.* Primary: 37E30, 37M25; Secondary: 58F13.
Key words and phrases. Dissipative systems, Weak dissipation, Nearly–integrable maps.

of the satellite. The outcoming model is described by a nearly–integrable dissipative system.
In this framework, we start the investigation of nearly–integrable dissipative systems by looking at a simple model problem, namely the dissipative standard map, which is ruled by two parameters, denoted as the dissipative (b) and the perturbing (ε) parameters. More precisely, we consider the mapping which generalizes the (conservative) Chirikov standard map ([9]) to the dissipative case as (see also [30]) described by the equations

$$\begin{aligned} y' &= by + c + \frac{\varepsilon}{2\pi}\ \sin(2\pi x) \\ x' &= x + y'\ , \end{aligned} \tag{1}$$

where $y \in \mathbf{R}$, $x \in [0,1)$, $c \in \mathbf{R}$, $b \in [0,1]$, $\varepsilon \in \mathbf{R}_+$; notice that the determinant of the jacobian of (1) is equal to b. In particular, the mapping is conservative whenever $b = 1$ and it is integrable whenever $\varepsilon = 0$. For $\varepsilon = 0$ one gets $y' = by + c$, providing that the trajectory $y = \alpha$ with $\alpha \equiv \frac{c}{1-b}$ is invariant for the unperturbed system.
In order to have a panorama of the dynamics generated by dissipative standard map–like systems, we consider also some generalizations of the mapping (1), obtained replacing the perturbation by a generic function of the form $\sin(2\pi mx) + d\sin(2\pi nx)$ for some integers m, n and some real coefficient d. To complete the scenario, we vary the frequency α of the unperturbed invariant trajectory, by selecting different rational and irrational frequencies. These dynamical systems present a wide class of behaviors as the parameters b and ε, as well as the indexes m and n or the frequency α, are varied. In particular, there might be essentially three types of attractors: invariant curves, periodic orbits and strange attractors (see also [5] with particular reference to the Appendix D).

The results available in the literature about periodic, invariant and strange attractors of the dissipative standard map are numerical and analytical. Let us mention that an exhaustive investigation of a dissipative representative model, the fattened Arnold map, is presented in [5]. The authors approach this study through analytical perturbation theory and numerical experiments, which provide a refined description of the dynamics, covering a wide spectrum of topics (from homoclinic and local bifurcations to *large* strange attractors, invariant circles, Arnold tongues, etc.).
Among the purely numerical studies, we quote the following which are closely related to the subject discussed in this paper. The extension of the fractal diagram to the dissipative case has been computed in [30] to investigate the behavior of stable periodic orbits and the occurrence of strange attractors; in particular, a numerical technique for the determination of periodic orbits in the dissipative standard map has been developed in [31] (notice that an arbitrary large number of periodic attractors may coexist, as shown in [12]). Concerning the quasi–periodic behavior in dissipative systems, a renormalization group analysis has been developed in [11] and a similar approach was adopted in [29] to study the transition from quasiperiodicity to chaos (see also [2]); it is interesting to mention that sometimes invariant circles may reappear after the breakup as it was shown in [17] for the Wilbrink map ([32]). Transition to chaos caused by overlapping of resonances has been investigated in [18].

Among the analytical results, let us mention that the persistence of an invariant (periodic or quasi–periodic) circle was proved in [26] using a fixed point theorem, provided the perturbing and dissipative parameters are sufficiently small. The existence of quasi–periodic invariant attractors is proved in [7] under smallness conditions on the parameters. The averaging method is developed in [27] on a two–frequency nearly–integrable system with a small dissipation, providing an approximate solution over a finite time interval. A geometrical approach to prove the existence of quasi–periodic orbits of a dissipative monotone twist map was developed in [23], while topological criteria for the existence of periodic attractors were investigated in [6].

Following the studies mentioned above, the present work aims to provide a global understanding of the dynamics through numerical and analytical techniques. In particular, we are interested in the investigation of the roles played by the dissipative and perturbing parameters, and their relation to periodic or quasi–periodic motions. In this respect, we start by implementing two numerical tools that are widely adopted in the domain of conservative systems. In particular, we decide to use the frequency analysis and a Fast Lyapunov Indicator adapted to the dissipative case, to which we refer as the *Differential Fast Lyapunov Indicator** (hereafter DFLI). In the conservative setting the first method allowed, for example, to make refined studies of the standard map ([22], [24]), while the second technique was very useful in determining the delicate transition from the Nekhoroshev regime of effective stability to the Chirikov regime of fast diffusion ([13], [16]). We remark that the two methods are strongly related: the first one provides the frequency characterizing an orbit, while the second, being linked to the derivative of the frequency, gives an insight on the properties of neighbouring trajectories.
We devote special attention to the occurrence of periodic orbit attractors as the parameters ε, b and the frequency α are varied. In particular, we analyze the parameter region close to the conservative framework, namely the *weakly dissipative regime*, which we let correspond to $b \geq 0.9$. In this context we study the behavior of periodic attractors (which seem to occur more often in the weakly dissipative regime, as showed by the DFLI analysis), providing examples which highlight why some periods are privileged by choosing a suitable frequency α and a suitable perturbing function. In the intermediate cases of moderate values of the perturbing and dissipative parameters, we still recover the same kinds of orbits, but the interplay between the dissipation and the perturbation is less evident and only a phenomenological or statistical description seems to be possible.

In the last part of the paper we provide an analytical determination of the frequency of motion, using a normal form analysis in the context of our dissipative nearly–integrable model problem (see also [8]). Explicit expansions are performed, using Mathematica, up to the fourth order of the Taylor development in the perturbing parameter (no constraint is required on the dissipative parameter). We remark that the formulae can be generalized to any order of the Taylor expansion. The normal form provides explicit formulae for the determination of the Taylor coefficients of the series expansion of the rotation number as a function of the perturbing parameter. Indeed, such formulae involve the occurrence of small divisors, in analogy to

*Color pictures showing the exploration of the dynamics of the dissipative standard map through DFLI analysis can be found at *http* : *//www.obs − nice.fr/elena/Images_dissi/images.html*

classical results obtained in the context of the conservative dynamics. A detailed investigation of the existence of invariant curve attractors through a Newton's method has been recently developed in [7]; compare also with [4]). An important issue investigated in [7] concerns the analysis of invariant curve attractors as the dissipative parameter tends to the conservative limit (see also [3] for the proof of the existence of quasi–periodic motions in the dissipative setting).

We remark that the methods developed in the present work can be generalized to higher dimensional mappings as well as to continuous systems.

This paper is organized as follows. The dynamical model is presented in section 2. We describe in section 3 the two techniques (Differential Fast Lyapunov Indicators and frequency analysis) which are used to investigate the dynamics of the dissipative standard mapping. The global dynamics of the mapping is studied in section 4, through the complementary use of the frequency analysis and of the DFLI. The computation of the dissipative normal form and the discussion of the analytical solution is presented in section 5. Some conclusions are reported in section 6.

2. **Set up of the mapping.** We consider the dissipative standard map described by the equations

$$\begin{aligned} y' &= by + c + \frac{\varepsilon}{2\pi}\, s(2\pi x) \\ x' &= x + y' \ , \end{aligned} \tag{2}$$

where $y \in \mathbf{R}$, $x \in [0,1)$, c is a real constant and $s(x)$ is a regular periodic function; the mapping depends on two parameters: $b \in \mathbf{R}_+$ is the *dissipative* parameter, while $\varepsilon \in \mathbf{R}_+$ is the *perturbing* parameter. We recall that a widely studied mapping belonging to the class (2) is the paradigmatic standard map, where the function $s(x)$ is defined as

$$s(x) = \sin(2\pi x) \ . \tag{3}$$

The determinant of the Jacobian associated to (2) amounts to b. Therefore, if $b = 1$ one recovers the *conservative* case, while for $0 < b < 1$ the system is (strictly) dissipative and if $b = 0$ one obtains the one–dimensional sine–circle–map:

$$x' = x + c + \varepsilon s(x) \ .$$

We first consider the conservative case ($b = 1$), where ε plays the role of the perturbing parameter, since for $\varepsilon = 0$ one gets an integrable mapping. We can label the conservative dynamics by fixing a *rotation number* (or *frequency*) defined as

$$\omega = \lim_{j\to\infty} \frac{x_j - x_0}{j} \ ,$$

where x_j denotes the j–th iterate with respect to the lift of the mapping (2) for $b = 1$. When the limit exists, we characterize an orbit by the corresponding rotation number ω. Indeed, for $c = 0$ and $\varepsilon = 0$, it is immediate to check that the frequency reduces to $\omega = y_0$. In particular, if ω is rational, say $\omega = \frac{p}{q}$ for some integers p and q, the corresponding trajectory is periodic with period q; if ω is irrational, the corresponding orbit describes an invariant curve. In the latter case, assuming that ω is diophantine (i.e., strongly non resonant), KAM theory ([19]) ensures that in the perturbed regime there still exists an invariant curve with frequency ω provided ε is sufficiently small. When ε reaches a critical value, say $\varepsilon_c = \varepsilon_c(\omega)$, the invariant curve breaks down through a loss of regularity. We remark that there is a wide

numerical evidence that for the standard map (defined by (3)) the last curve to disappear (in the interval $(0,1)$) is that with frequency equal to the golden ratio $\frac{\sqrt{5}-1}{2}$.

Let us turn to the dissipative case ($b \neq 1$) and let us define the auxiliary quantity α as

$$\alpha \equiv \frac{c}{1-b} \; ; \tag{4}$$

it is immediate to check that for $\varepsilon = 0$ the trajectory $\{y = \alpha\} \times T^1$ is invariant (T^1 denotes the standard one–dimensional torus). In fact, the condition $y' = y$ implies $\alpha = b\alpha + c$, which coincides with (4). Notice that when $b = 1$, equation (4) implies that $c = \alpha(1-b) = 0$, as it was assumed before for the conservative case. Indeed, to vary α is equivalent to change the *drift parameter* c; the existence of a quasi–periodic solution with frequency ω is proved in [7] by setting $c \equiv c_0(b) + c_1(\varepsilon, b)$, such that $c_0(b) \equiv \omega(1-b) \to 0$ as $b \to 0$, while $c_1(\varepsilon, b)$ is small with ε and tends to zero as b goes to zero.
The trajectory $\{y = \alpha\} \times T^1$ can represent a periodic orbit or an invariant curve, according to the rational or irrational character of α. In this context, the topological stability was investigated in [26], independently of the preservation of the nature of the dynamics. Based on a fixed point theorem, the persistence of an invariant (periodic or quasi–periodic) circle is proved in [26] under suitable (smallness) conditions on the perturbing and dissipative parameters.

The major goal of the present work is to discriminate among the different roles played by the choice of the function $s(x)$, as well as by the frequency α, as the parameters (ε, b) and the initial conditions are varied. Since (3) might provide only a partial scenario, we select several perturbing functions with one or two harmonics (cases $(A) - (E)$ below), plus a sample (F) which admits a full Fourier spectrum:

(A) $s(2\pi x) = \sin(2\pi x)$;
(B) $s(2\pi x) = \sin(2\pi x \cdot 3)$;
(C) $s(2\pi x) = \sin(2\pi x \cdot 5)$;
(D) $s(2\pi x) = \sin(2\pi x) + \frac{1}{3}\sin(2\pi x \cdot 3)$;
(E) $s(2\pi x) = \sin(2\pi x) + \frac{1}{20}\sin(2\pi x \cdot 5)$;
(F) $s(2\pi x) = \frac{\sin(2\pi x)}{\cos(2\pi x)+1.4}$.

Similarly we vary α, motivated by the fact that the dynamics of the conservative case is strongly dependent on the degree of irrationality (the so–called *diophantine condition*) of the frequency; therefore, we decide to consider for each mapping $(A)-(F)$ different values of α. In this work we are mainly concerned with the numbers $\frac{\sqrt{5}-1}{2}$, $\frac{1}{2}$, $\frac{1}{3}$, though we performed the experiments on a larger set of frequencies, including diophantine irrationals[†] like $[1,3,4,1^\infty]$, $[6,1,7,1,3,1,266,1,3,1^\infty]$, as well as rational frequencies like $\frac{3}{5}$, $\frac{5}{8}$, $\frac{2}{3}$, 1, $\frac{3}{2}$, 2, etc.
The first question to be clarified is the type of dynamics which arises from the evolution of the mapping (2). Taking any of the maps $(A) - (F)$ combined with any of the previous values of α, it is evident that only three kinds of attractors are present: periodic orbits, invariant curves, strange attractors; the largest Lyapunov

[†]The continued fraction representation is denoted as $\alpha \equiv [a_1, a_2, ..., a_N, ...]$ for $a_k \in \mathbf{Z}_+$ ($k \geq 1$), standing for $\alpha = \frac{1}{a_1 + \frac{1}{a_2 + \frac{1}{a_3 + \cdots}}}$; the notation 1^∞ denotes an infinite tail of ones.

exponent is, respectively, negative, equal to zero, positive. To give concrete examples of the three attractors, we show in Figure 1*a* a strange attractor (mapping (D) with $\alpha = \frac{\sqrt{5}-1}{2}$), while an invariant curve and a periodic orbit attractors are provided in Figure 1*b* (mapping (A) with $\alpha = \frac{\sqrt{5}-1}{2}$).

3. **The DFLI and frequency analysis.**

3.1. **Differential Fast Lyapunov Indicator.** In order to perform a global analysis of conservative systems, Froeschlé et al. ([15]) introduced a tool strictly related to the computation of the largest Lyapunov exponent: the Fast Lyapunov Indicator (hereafter FLI). The definition of the FLI is based on the simple observation that in order to discriminate the dynamical behaviour of an orbit, it is sufficient to compute the norm of the tangent vector over a finite interval of time. Beside being computationally faster than the standard Lyapunov exponent, the FLI method allows to discriminate between regular invariant tori and regular resonant tori (for more details we refer the reader to [13], [16]).
Let us denote by $\tilde{M}$ the lift of the mapping (2). Let $z(0) \equiv (y(0), x(0))$ be the initial condition and let $v(0) \equiv (v_y(0), v_x(0))$ be an initial vector with norm equal to one. For a fixed time $T > 0$ we define the FLI function as

$$\overline{FLI}(z(0), v(0), T) \equiv \sup_{0<t\leq T} \log \|v(t)\| \ , \tag{5}$$

where $\|\cdot\|$ denotes the Euclidean norm in $\mathbf{R}^2$ and $v(t)$ is the solution of the system

$$\begin{aligned} z(t+1) &= \tilde{M}(z(t)) \\ v(t+1) &= \frac{\partial \tilde{M}}{\partial z}(z(t))v(t) \end{aligned}$$

with initial data $z(0)$, $v(0)$. We remark that the computation of the supremum of the logarithm of the vector has been introduced in order to get rid of the oscillations of $||v(t))||$; for simplicity let us denote by $FLI(t)$ the $\log \|v(t)\|$. In the unperturbed conservative case (see (2) with $\varepsilon = 0$, $b = 1$) the FLI as a function of time takes the form

$$FLI(z(0), v(0), t) = \frac{1}{2}\log(v_y(0)^2 + (tv_y(0) + v_x(0))^2) \ ;$$

it appears clearly that, unless $v_y(0) = 0$, the FLI grows as $\log(t)$ and that all orbits will have the same FLI at a given time t when choosing the same initial vector $v(0)$. In the unperturbed dissipative case (see (2) with $\varepsilon = 0$, $b < 1$) the evolution of the vector $v(0)$ is given by

$$\begin{aligned} v_y(t) &= b^t v_y(0) \\ v_x(t) &= (\frac{b - b^{t+1}}{1-b})v_y(0) + v_x(0) \ ; \end{aligned} \tag{6}$$

therefore, for a sufficiently large time the FLI behaves as

$$FLI(z(0), v(0), t) \simeq \log(|\frac{b}{1-b}v_y(0) + v_x(0)|) \ . \tag{7}$$

For an unperturbed curve attractor the largest Lyapunov exponent is equal to zero, but this situation may not be reflected by the corresponding FLI, since according to (7) it can take any value in the interval $[\log(|v_x(0)|), +\infty)$ for $0 \leq b < 1$. By continuity the same problem holds for ε different from zero. As a consequence, we might not be able to differentiate between an invariant curve attractor and a strange

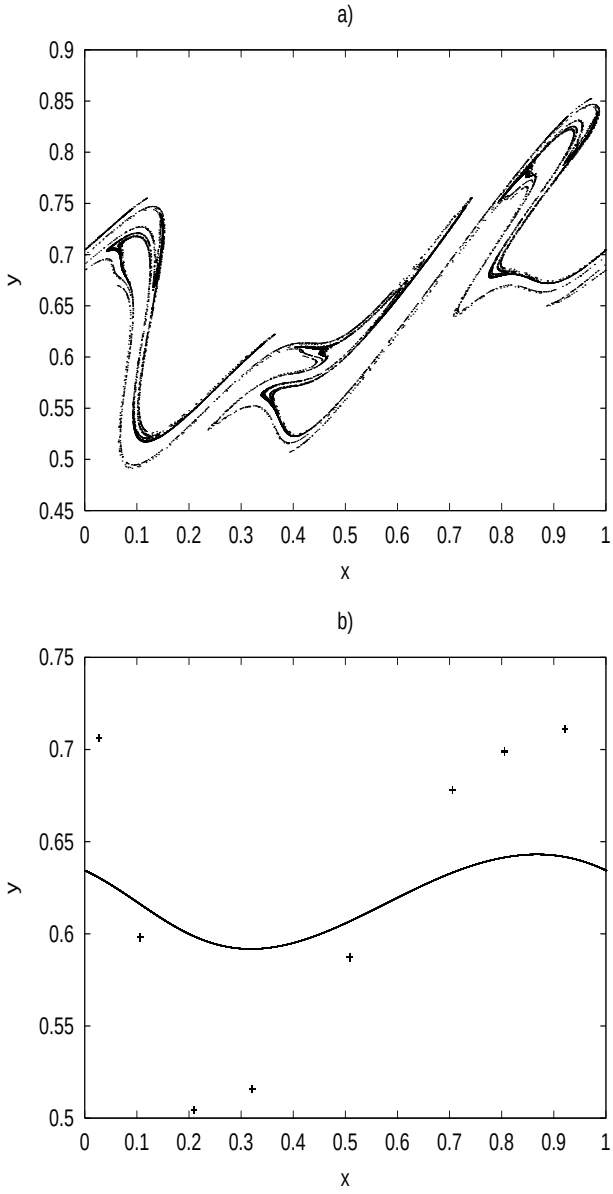

FIGURE 1. Characteristic attractors of the dissipative standard map for $\alpha = (\sqrt{5}-1)/2$ and initial conditions $y_0 = 5$, $x_0 = 0$. *a*) Mapping (D), $b = 0.72699$, $\varepsilon = 0.9$. *b*) Mapping (A), $b = 0.3$, $\varepsilon = 0.2$ for the invariant curve attractor and $b = 0.4$, $\varepsilon = 0.9$ for the periodic orbit attractor.

attractor, whose FLI is intrinsically positive. Due to the fact that the FLI may give misleading results in the dissipative contest, we introduce a different indicator, the DFLI_0, defined as

$$DFLI_0(z(0), v(0), t) \equiv FLI(z(0), v(0), 2t) - FLI(z(0), v(0), t) \ . \tag{8}$$

From (7) in the unperturbed dissipative case the DFLI_0 turns out to be close to zero for any value of b and for a sufficiently large t. By continuity for $\varepsilon \neq 0$ the DFLI_0 remains zero for curve attractors, it is negative for periodic orbit attractors and it is positive for chaotic attractors as well as their corresponding largest Lyapunov exponent.
Let us now denote for simplicity the norm of the vector $v(t)$ computed from $z(0)$ for an initial vector $v(0)$ as $w_t(z(0), v(0))$. We remark that:

$$w_{2t}(z(0), v(0)) = w_t(z'(0), v'(0)) \cdot w_t(z(0), v(0)) \ ,$$

where $z'(0) = z(t)$ and $v'(0) = v(t)/||v(t)||$. From (8) we obtain

$$DFLI_0(z(0), v(0), t) = FLI(z'(0), v'(0), t) \ ;$$

the above expression indicates that the DFLI_0 is nothing but the FLI computed from an initial vector, which evolved long enough to become parallel to the direction of maximal expansion corresponding to the maximum Lyapunov exponent. In the unperturbed dissipative case the DFLI_0 corresponds to the computation of the FLI starting from the vector $(v_y, v_x) = (0, 1)$. Since such vector remains constant with time (see (6)), the DFLI_0 is identically equal to zero. It turns out that the DFLI_0 corresponds to the largest Lyapunov exponent, computed after a transition time allowing the vector to become aligned with the direction of maximal expansion.
In the conservative case the spirit of the computation of the $\overline{FLI}$ is at the opposite, since, for regualar motion it gives information thanks to the transition of the initial vector toward a direction tangent to the support of the orbit. In the chaotic case, the vector becomes rapidly aligned with the direction of maximal expansion and its exponential increase allows to detect very quickly the associated dynamic.

Let us now discuss the technical point of the introduction of the supremum in (5). In order to kill the oscillations of the norm of the vector v a supremum in equation (5) has been introduced. For dissipative systems the problem of the oscillations still remains and, in addition, we have to take into account the fact that $\log \|v(t)\|$ is negative for periodic attractors. Therefore, from a practical point of view, for some $T > 0$, we computed the differential fast Lyapunov indicator, DFLI, as

$$DFLI(T) = G_{2T}(F(t)) - G_T(F(t)) \ ,$$

where $F(t) = \log(||v(t)||)$ and

$$G_\tau(F(t)) = \sup_{0 \le t \le \tau} F(t) \qquad \text{if } F(\tau) \ge 0 \tag{9}$$

$$G_\tau(F(t)) = \inf_{0 \le t \le \tau} F(t) \qquad \text{if } F(\tau) < 0 \ . \tag{10}$$

Figure 2 shows the evolution of the DFLI with respect to time for the three orbits displayed in Figure 1. Here and in the following computations we consider the initial vector $v(0) = (1, 0)$. Let us remark that the introduction of the DFLI is relevant for dissipative systems, whose dynamics must have evolved sufficiently long to be close to an attractor. To this end, we introduced in our computation a preliminary transient period (typically of 10^4 iterations).

3.2. **Frequency analysis.** A widely used technique for the investigation of conservative systems is the so–called frequency map analysis ([22]), which is based on the investigation of the behavior of the frequency with respect to the parameters. This method was largely popularized by Laskar et al. ([20], [22]) and successfully

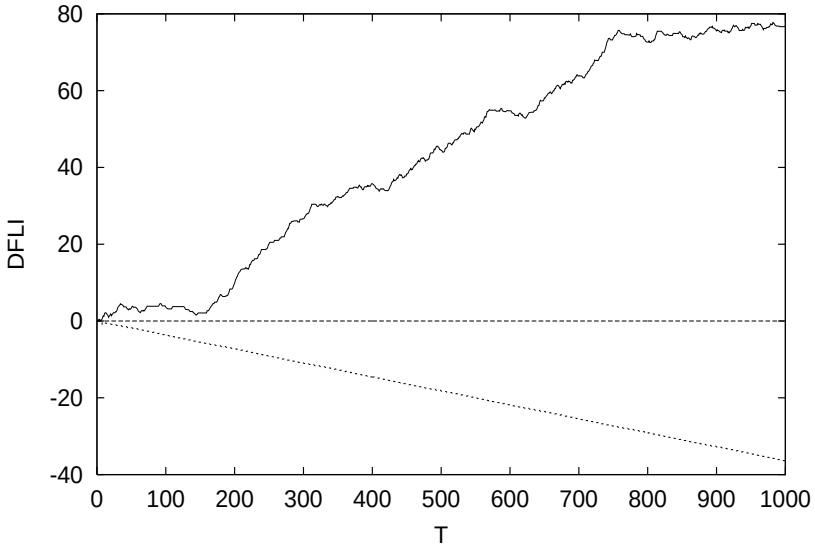

FIGURE 2. Evolution of the DFLI with time for the three orbits of Figure 1. The positive DFLI corresponds to the strange attractor of Figure 1*a*, the DFLI close to zero corresponds to the invariant curve, while the DFLI lower than zero is associated to the periodic orbit attractor.

used to refine the analysis of Hamiltonian systems ([22], [24]). We will use a simple technique, introduced in [24], related to the continued fraction development of real numbers. Given a conservative 2–dimensional mapping M, we consider the n–th iterate point $P_n = M^n(P_0) \equiv (x_n, y_n)$ on an invariant curve with frequency β. Over N iterations of the mapping M, we compute in the set $(P_1, ..., P_N)$ the nearest neighbor to P_0 and we denote by n_1 its index; next, we define the integer p_1, by the relation:

$$n_1\beta = p_1 + \epsilon_1 \ ,$$

where ϵ_1 is a small quantity. In other words, p_1 counts the number of revolutions around the invariant curve, so that β can be approximated by the ratio p_1/n_1. By increasing the number N of iterations, we get better approximations, so that the errors ϵ_i satisfy the following sequence of inequalities, $\epsilon_1 > \epsilon_2 .... > \epsilon_k$ implying that

$$|n_1\beta - p_1| > |n_2\beta - p_2| > ... > |n_k\beta - p_k| \ ,$$

where the n_i's are the smallest integers satisfying the above inequalities. For $n_1 = 1$, the sequence p_k/n_k coincides with the expansion in continued fractions of β. We know from a theorem of Lagrange that such expansion provides the best approximation of the number β. We also know that $\epsilon_k < 1/(n_k n_{k+1})$ and that $n_{k+1} > a_k n_k + n_{k-1}$, where a_k is the k–th term of the expansion in continued fractions. These relations allow to get an estimate of the precision, namely the price we have to pay in order to obtain the next nearest neighbor of P_0. In this way, we can evaluate the rotation number by the simple formula $\beta = \lim_{k\to\infty} \frac{p_k}{n_k}$. In order to apply this method to the dissipative case, it is essential that the starting point P_0

is close to the attractor; therefore, in the numerical experiments presented in this paper, we have always considered a transition of 10^4 iterations before defining the initial point P_0.

It is interesting to note that applying this procedure to the analysis of an invariant curve attractor (with frequency β) of the dissipative case, we obtain a sequence of approximants p_i/n_i corresponding to the terms of the continued fraction development of β, as it happens in the conservative case.
However, the procedure can fail for very weak dissipations, since the transition to the attractor may be very long and 10^4 iterations may not be sufficient to get close to the attractor. Since we do not know a priori the right transition time, we can try to compute the frequency as the limit of a sequence of values ω_i obtained on successive intervals of time. Along this line, we propose the following procedure: consider N iterations of the mapping and define $P_{0,1}$ as the N–th iterate with associated frequency ω_1. Iterate again the mapping up to a time $T = 2N$ with ending point $P_{0,2} = P_{2N}$ and corresponding frequency ω_2. Proceed in this way up to the convergence (within a finite precision) of the set of the ω_i's and let ω be the numerical limit of the sequence $\{\omega_i\}$.
As an example, consider the mapping (A) with $\alpha = \frac{\sqrt{5}-1}{2}$; Figure 3 shows the evolution of the frequencies $\omega \equiv \omega_i$ as a function of $N \times i$ (with $N = 100$ and $i = 1, ..., 100$) for $b = 0.999$, $\varepsilon = 0.1$, $x_0 = 0$ and a set of 9 initial conditions regularly spaced in y_0, from $y_0 = 0.1$ to $y_0 = 0.9$. We observe that, apart for the case $y_0 = 0.5$, the other sequences converge to $\omega = \alpha$ with a speed depending on y_0. If we consider the case $\varepsilon = 0$ the convergence to the attractor $y = \alpha$ depends on the initial condition y_0 and on b through the relation

$$y_n = y_0 b^n + \alpha(1 - b^n) \ .$$

For small values of ε, this law is satisfied with the exception of the orbit starting at $y_0 = 0.5$, for which we find a very robust periodic orbit attractor with frequency $\omega = \frac{1}{2}$, surviving under dissipation from the conservative regime.

3.3. **On the complementarity of the DFLI and frequency analysis.** In order to give evidence of the different roles played by the DFLI and frequency analysis, it is convenient to study a concrete example. More precisely, consider the mapping (D) with $\alpha = \frac{\sqrt{5}-1}{2}$, $b = 0.5$ and initial conditions $y_0 = 5$, $x_0 = 0$. To investigate the dependence of the frequency and of the DFLI with respect to ε, we analyze a set of 1000 orbits regularly spaced in ε with $0 < \varepsilon < 1$. As explained before, a transition of 10^4 iterations has always been considered in order to get close to the attractor; after the transient, we perform $T = 1000$ iterations (the initial vector is always set to $v(0) = (1, 0)$).
Figure 4 shows the variation of ω and of the $DFLI$ with respect to ε. The frequency (Figure 4*a*) monotonically increases from $\omega = \alpha$ to $\omega = 5/8$ when ε varies from 0 to about 0.3. Then we observe a *"plateau"* of frequency 5/8 up to about $\varepsilon = 0.4$. Let us remark that 5/8 is one of the low order terms of the development in continued fractions of α. Up to $\varepsilon \simeq 0.3$ we meet invariant curve attractors (the corresponding DFLI is zero, see Figure 4*b*), while between 0.3 and 0.4 we detect periodic orbit attractors (the corresponding DFLI is negative). Let us remark that there is an interesting correspondence with the behavior of the frequency in Hamiltonian systems, where ω changes monotonically or shows *"plateau"* when representing, respectively, invariant KAM tori or resonant islands. The difference

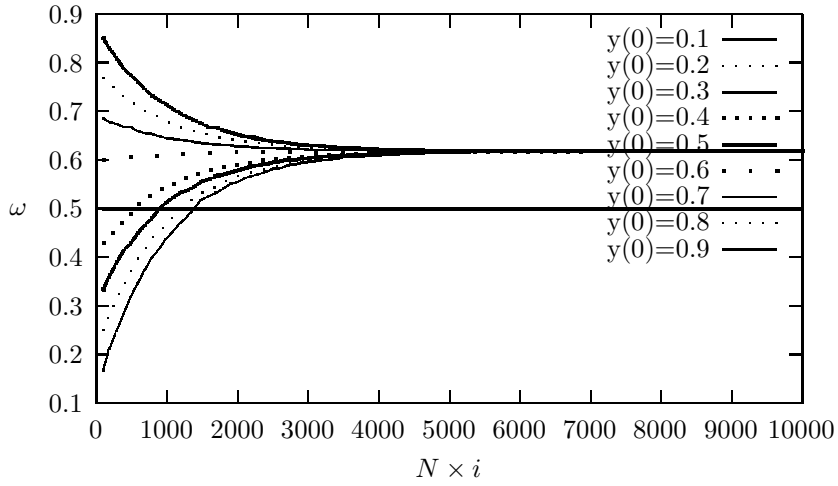

FIGURE 3. Mapping (A) with $\alpha = \frac{\sqrt{5}-1}{2}$. Evolution of the frequencies ω_i as a function of $N \times i$, $N = 100$ and $i = 1, ..., 100$ for $b = 0.999$, $\varepsilon = 0.1$, $x_0 = 0$ and a set of 9 initial conditions regularly spaced in $y(0) \equiv y_0$, from $y_0 = 0.1$ to $y_0 = 0.9$. We notice that the initial values of the frequencies ω correspond to the y_0 values labelling the different curves.

is that in the Hamiltonian case this behavior occurs as a function of the initial condition, while in the dissipative case it occurs as a function of the perturbing parameter.

For ε running from 0.4 to 0.45 the DFLI is almost everywhere positive, but with some sparse negative values corresponding to periodic orbit attractors (Figure 4*b*). Such periodic orbit attractors can be detected as small *"plateau"* by means of frequency analysis implemented on a zooming of the above region. At the present resolution, we observe in this parameter region (Figure 4*a*) a noisy variation of the frequency. For larger values of ε, up to $\varepsilon \simeq 0.93$, we have a big region of constant frequency $\omega = \frac{2}{3}$. The corresponding DFLI remains negative up to $\varepsilon = 0.9$, after which we enter a region of strange attractors with positive DFLI having rational frequency. Notice that like for the Hamiltonian chaos, the frequency is not defined for strange attractors. We remark that for $\varepsilon = 0.92$ one finds a strange attractor made of three pieces, for which the frequency is rational with period 3; in this case the complementary use of the frequency analysis and of the DFLI is essential, since without the DFLI the diagnostic of the dynamics would provide misleading results. For $\varepsilon > 0.93$ we have again a noisy variation of the frequency with positive DFLI, corresponding to standard strange attractors, i.e. one–piece attractors like that presented in Figure 1*a*.

This example shows that the parallel implementation of frequency analysis and of the DFLI allows to distinguish clearly among the different kinds of attractors. A similar analysis holds when looking at the variation of the frequency and of the DFLI for a fixed value of ε and for a set of orbits regularly spaced over a grid in the dissipative parameter b.

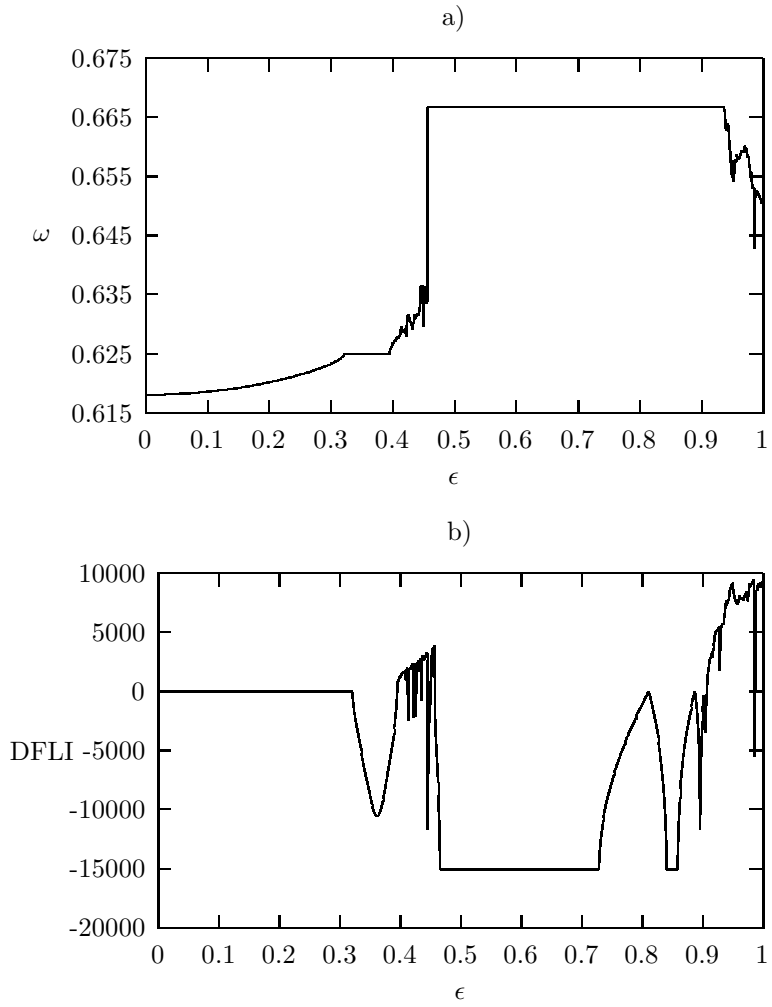

FIGURE 4. Mapping (D) with $\alpha = \frac{\sqrt{5}-1}{2}$, $b = 0.5$, $y_0 = 5$, $x_0 = 0$. Variation of ω (a) and of the DFLI (b) as a function of ε for a set of 1000 orbits regularly spaced in ε with $0 < \varepsilon < 1$.

4. **Global dynamics of the dissipative map.** We proceed to implement the frequency analysis and the DFLI technique, in order to explore the dynamics as the perturbing and dissipative parameters are varied. In particular we draw some conclusions on the occurrence of periodic orbit attractors, their link with the definition of the mapping (i.e., the explicit form of the function $s(x)$) and with the choice of the frequency α. Particular attention is devoted to the study of the weakly dissipative regime occurring for high values of the dissipative parameter, say $b > 0.9$.

4.1. **The Frequency analysis.** The mapping (2) depends on the parameters ε, b: their variation provokes several behaviors, from integrable to non–integrable dynamics as well as from conservative to dissipative regimes. In order to investigate the effect of the simultaneous variation of the dissipative and perturbing parameters,

we adopt the powerful tool represented by the frequency analysis. More precisely, we draw the curve $\omega = \omega(b)$ for different values of ε in the interval $[0, 1]$ with step–size 0.1. Exhaustive examples are provided by the one/two frequency mappings (A), (D) and by the irrational/rational rotation numbers $\frac{\sqrt{5}-1}{2}$, $\frac{1}{3}$. The outcome of this technique allows to recognize the different kinds of attractors (invariant, periodic or strange) and it gives information on their behavior as functions of b and ε. The results will show that invariant curves occur more frequently for small values of ε, while periodic and strange attractors appear more often as the non–integrability gets larger.

We start by considering the mapping (A) with $\alpha \equiv \frac{\sqrt{5}-1}{2}$ (initial conditions $y_0 = 1$, $x_0 = 0$). In Figure 5a) the lower curve corresponds to $\varepsilon = 0.1$, while the upper curve is computed taking $\varepsilon = 0.9$. The inspection of this figure shows that for low values of ε, almost all attractors are invariant curves for any value of the dissipation in the interval $[0, 1]$. Periodic orbits appear at higher values of ε: a significant region of periodic orbit attractors emerges at $\varepsilon = 0.8$ around $b = 0.2$ and it becomes even larger at $\varepsilon = 0.9$ around $b = 0.3$. The existence of so many invariant curve attractors is definitely ruled by the choice of the irrational frequency α. Indeed, this situation is reversed when α is a rational number as shown in Figure 5b), where almost everywhere we find a dominant periodic attractor with period $\frac{1}{3}$; the dissipative parameter region where this attractor dominates is shown to extend as the perturbing parameter gets larger.

Let us see what happens taking the two frequency map (D); the irrational case with $\alpha = \frac{\sqrt{5}-1}{2}$ is analyzed in Figure 5c), where the size of the periodic regime as well as that of the strange attractor behavior is again larger as ε increases. In this case there are two dominant periodic orbit attractors with periods, respectively, 1 and 3; indeed, this is consistent with the fact that 1 and 3 are also the main harmonics appearing in the definition of the mapping (D) and with the fact that the golden mean frequency does not *force* toward a given resonance, being equal to a strongly irrational number. On the contrary, Figure 5d) shows the case $\alpha = \frac{1}{3}$: almost all trajectories are attracted toward the periodic attractor with frequency $\frac{1}{3}$. At $\varepsilon = 0.8$ there appear a significative region of strange attractors; such region is magnified at $\varepsilon = 0.9$ where also a periodic orbit of period 4 is shown to appear around $b = 0.5$.

4.2. **The DFLI analysis.** The DFLI technique allows to discriminate the different dynamics associated to the dissipative mapping and it is used as a complementary investigation to the frequency analysis of the previous paragraph, providing the variation of the frequency as a function of the dissipation for discrete values of ε. We represent with a color scale the value of the DFLI in the $b - \varepsilon$ or $b - y_0$ plane (y_0 denoting the initial condition). Though not yielding the explicit value of the frequency, such analysis still provides the discrimination among the different attractors (invariant, periodic or strange). In particular, the DFLI charts allow to give a striking visualization of the dynamics by providing information on the transition between the different regimes. More precisely, the $b - \varepsilon$ chart provides a geography of the attractors as a function of the dissipative and perturbing parameters, while the $b - y_0$ chart is useful to explore the dependence on the initial condition and the eventual occurrence of simultaneous attractors as the initial condition is varied; we refer to [5], [12] for a discussion of the the coexistence of attractors (periodic, quasi–periodic or strange).

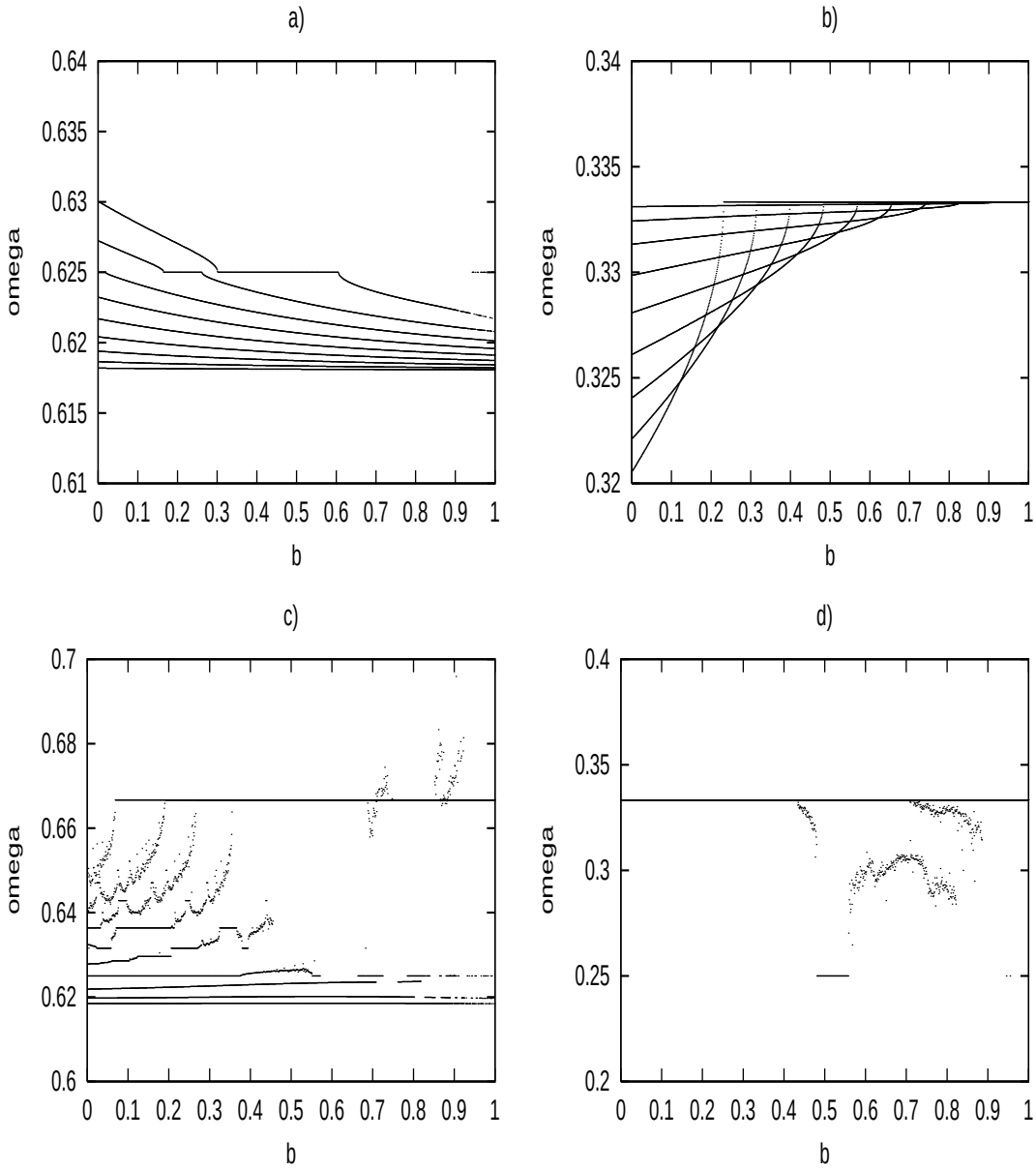

FIGURE 5. Frequency analysis showing the curve $\omega = \omega(b)$ for different values of ε with step–size 0.1. *a*) Mapping (A) with $\alpha = \frac{\sqrt{5}-1}{2}$ ($y_0 = 1$, $x_0 = 0$) from $\varepsilon = 0.1$ (lower curve) to $\varepsilon = 0.9$ (upper curve). *b*) Mapping (A) with $\alpha = \frac{1}{3}$ ($y_0 = 1$, $x_0 = 0$) from $\varepsilon = 0.1$ (upper curve) to $\varepsilon = 0.9$ (lower curve). *c*) Mapping (D) with $\alpha = \frac{\sqrt{5}-1}{2}$ ($y_0 = 1$, $x_0 = 0$) from $\varepsilon = 0.1$ (lower curve) to $\varepsilon = 0.9$ (upper curve). *d*) Mapping (D) with $\alpha = \frac{1}{3}$ ($y_0 = 1$, $x_0 = 0$).

The practical implementation is hereafter described. We compute some pictures corresponding to grids of 500×500 initial values of b and ε regularly spaced in the interval $[0.01 : 1]$ for the initial conditions $y_0 = 5$ and $x_0 = 0$; the time parameter entering the definition of the $DFLI$ is always set to $T = 10^3$, after a transient of 10^4 iterations. Another set of pictures is obtained by computing grids of 500×500 initial conditions of b and y_0 in the intervals, respectively, $[0.01 : 1]$ and $[0.01 : 10]$ with $\varepsilon = 0.9$ and $x_0 = 0$. We have represented in a grey-scale the values

$$sgn(DFLI(2T))\ \log_{10}(|DFLI(2T)| + 1)$$

with the following interpretation:

- invariant curve attractors are denoted by grey: the $DFLI$ values are close to zero;
- strange attractors are labeled by bright grey to white: the $DFLI$ values are positive;
- periodic orbit attractors are denoted by colors going from dark grey to black .

A gallery of color pictures encompassing different mappings and a wide choice of rotation numbers is available at $http://www.obs-nice.fr/elena/Images\_dissi/images.html$.
The complexity of the dynamics is well represented by the two-frequency mapping (D) with rotation number $\alpha = \frac{\sqrt{5}-1}{2}$ (see Figure 6, top panel): a large region of invariant curve attractors appears up to $\varepsilon \simeq 0.36$; next, a strip of periodic attractors is evident for values of ε around 0.4. For greater values of ε a big region of periodic attractors is surrounded by two large zones of strange attractors. Notice that the bright regions of strange attractors are interspersed by periodic orbit attractors. In particular, in this as well as other examples, we found that strange attractors always originate from a region of periodic orbit attractors. A cross check of this statement is obtained looking back at Figure 4, where we infer that the strange attractor regimes always occur after plateaus of the frequency analysis curve. Notice that in the right part of the top panel of Figure 6 the picture is resembling Arnold's tongues (see [5]): such trajectories correspond to periodic orbit attractors, which play a dominant role in the region $b \geq 0.9$, to which we refer as the *weakly dissipative regime*. This behavior was found also in many other examples with different mappings and rotation numbers. In a few cases we detected some regions (usually small) of the chart filled by strange attractors. Figure 6, bottom panel, shows that for a fixed value of b the basin of attraction is typically unique, with the exception of the interval approximately given by $0.65 < b < 0.9$, where different initial conditions can be attracted either by a periodic orbit or by a strange attractor. Indeed, as already remarked in [12], for standard map–like systems there might coexist several periodic attractors.
We remark that the transition from periodic orbits to invariant curve attractors takes place for very small changes of the parameters, thus showing a phenomenon known as *crises*, denoting a sensitive dependence on parameters. This behavior is evident from the abrupt change of colors in the $DFLI$ chart, providing the transition between different kinds of attractors.

4.3. **On the occurrence of periodic orbit attractors.** The role of periodic orbits is relevant both from the physical and dynamical point of view. In the first case, periodic trajectories correspond to resonances which frequently occur in physical situations; in the latter case, periodic orbits can be conveniently used as

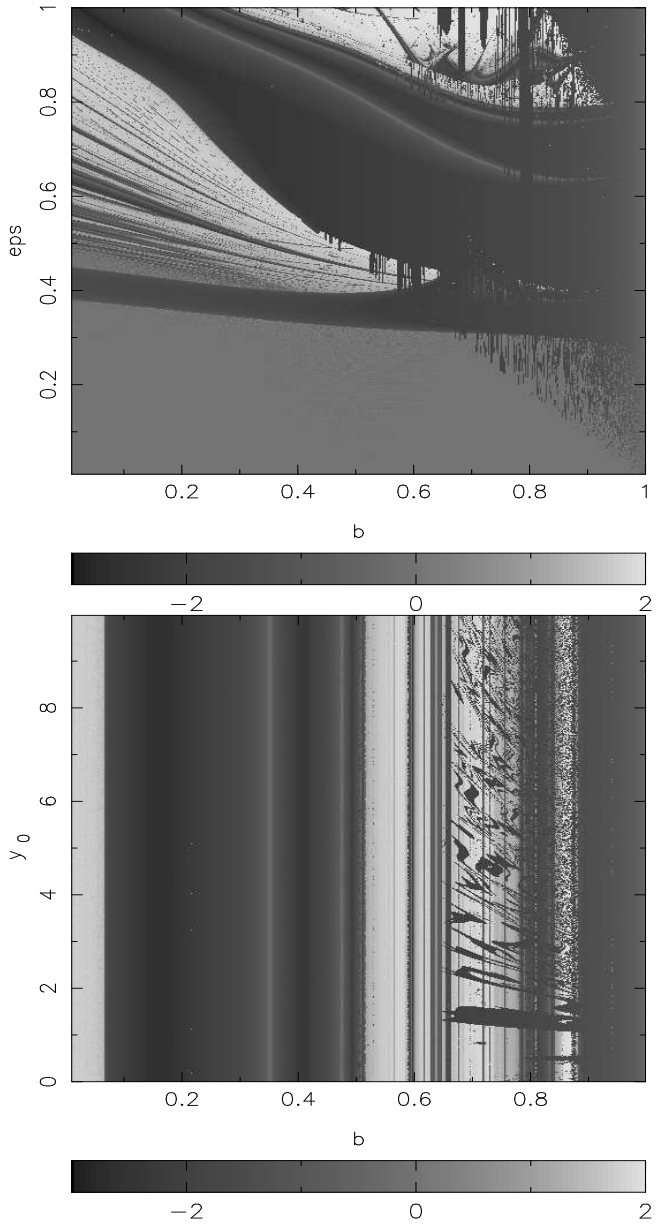

FIGURE 6. Mapping (D) with $\alpha = \frac{\sqrt{5}-1}{2}$. Top panel: DFLI picture of 500×500 initial values of b and ε regularly spaced in the interval $[0.01 : 1]$ for the initial conditions $y_0 = 5$ and $x_0 = 0$. Bottom panel: DFLI picture of 500×500 initial conditions of b and y_0 in the intervals, respectively, $[0.01 : 1]$ and $[0.01 : 10]$ with $\varepsilon = 0.9$ and $x_0 = 0$. The color version of this figure is available at *http* : $//www.obs - nice.fr/elena/Images\_dissi/images.html$.

approximants to invariant quasi–periodic motions. With this motivation, we intend to investigate the occurrence of attractors of periodic type as the parameters ε, b are varied. In other words, we are interested to know in which situations some periodic orbit attractors are privileged, in the sense that they occur more frequently than others; moreover, we want to explore the relationship between the periods of the periodic attractors and the form of the mapping (i.e., the function $s(x)$) as well as the link with the frequency α. To this end, we perform some experiments based on frequency analysis, combined with a complementary computation which specifies the period of the attractor (whenever the dynamics is represented by a periodic attractor). The results are reported in Tables 1, 2, 3, which are computed, for a fixed value of α, along the following steps:

i) let ε assume the values $0.1 \cdot k$ for $k = 1, ..., 9$;
ii) fix $x_0 = 0$ and let y_0 vary between 0 and 9.9 with step–size 0.1;
iii) let $b = 0.1$; compute the frequency of the attractor, say ω, and check whether it is a rational number, say $\frac{p}{q}$ with $p, q \in \mathbf{Z}_+$. In such case, q is the period and we count the number of occurrences of periodic orbits with period q for all values of ε indicated at point *i*);
iv) repeat the same computation for $b = 0.5$ and $b = 0.9$.

The analysis of Tables 1, 2, 3 leads to the following conclusions, which provide information on the relationship between the basic period, the value of α and the explicit form of the mapping:

1) the occurrence of a periodic orbit with given period q is strongly determined by the value of α and by the form $s(x)$ of the mapping. In particular, if $\alpha = \frac{p}{q}$, then it is very likely that the dynamics privileges attractors with period q (compare with Tables 2 and 3). Similarly, if $s(x) = \sin(2\pi x \cdot q)$, then the dynamics is most likely attracted by a periodic orbit with period q (compare, for example, the occurrence of the period-3 orbit for the mapping (B) and the period-5 orbit for the mapping (C) in Table 1);
2) for small values of b the role of α is prevalent with respect to that of $s(x)$; for large values of b, both α and $s(x)$ play a dominant role in the selection of the periodic attractors (compare, e.g., with Table 3). Indeed, most of the periodic orbit attractors can be found for large b if ε is small or for large ε if b is small;
3) periodic orbit attractors with small period occur more frequently, while large period attractors are very uncommon;
4) when we let b increase, we notice the birth of new periodic orbits with different periods (see the cases $b = 0.9$); in particular, the flowership of different periodic attractors takes place in the weakly dissipative regime that we are going to study in the next section.

4.4. **The weakly dissipative regime.** A particular interest is performed by the weakly dissipative regime, where the dissipation is rather feeble, but still of significant influence on the dynamics. To this end, we investigate the parameter region $b \in [0.9, 1]$, devoting attention to the behavior and occurrence of periodic attractors labeled by a rational frequency, say $\omega = \frac{p}{q}$ for $p, q \in \mathbf{Z}_+$. As in the previous section, we focus on the role of the mapping $s(x)$ and of the choice of α. More precisely, we consider the mapping $s(x) = \sin(3x)$ with $\alpha = \frac{1}{2}$ and we count the number of

	(A)	(B)	(C)	(D)	(E)	(F)
$b = 0.1$		3#700	5#700	3#100	8#300	3#100
			8#1	8#100		5#100
$b = 0.5$	8#100	3#800	5#900	3#500	8#200	2#1
						3#102
						5#100
						8#101
$b = 0.9$	1#242	1#124	1#56	1#288	1#245	1#139
	2#4	2#2	5#841	2#7	2#4	2#240
	3#7	3#743	10#3	3#383	3#24	3#246
		6#1		7#2	5#106	4#1
				8#37	8#63	5#88
						13#1

TABLE 1. Results for $\alpha = \frac{\sqrt{5}-1}{2}$. The notation "$q\#n$" stands for "the periodic orbit with period q occurs n times". We limited to consider $q \leq 10$.

	(A)	(B)	(C)	(D)	(E)	(F)
$b = 0.1$	1#900	1#900	1#824	1#900	1#900	1#900
$b = 0.5$	1#900	1#900	1#872	1#900	1#900	1#900
			5#28			
$b = 0.9$	1#900	1#725	1#654	1#896	1#900	1#894
		3#173	5#243	3#4		2#5
		6#2	10#3			3#1

TABLE 2. Results for $\alpha = 1$. The notation "$q\#n$" stands for "the periodic orbit with period q occurs n times". We limited to consider $q \leq 10$.

occurrences (on a semi–logarithmic scale) of a periodic orbit attractor of period q as ε varies (see Figure 7a)). The rotation number is computed taking 100 initial conditions ($x_0 = 0$ and y_0 in the interval $[0, 10)$) for each value of b between 0.901 and 0.999 with step–size 0.001, while ε takes the discrete values 0.1, 0.2, ..., 0.9.

The results show that there is a marked competition between the frequency $q = 3$ (equal to the harmonic of the mapping $s(x)$) and the frequency $q = 2$ (due to the choice of $\alpha = \frac{1}{2}$).
The occurrence of the frequency $q = 3$ increases from $\varepsilon = 0.1$ to $\varepsilon = 0.9$, which means that the effect of the choice of the mapping is stronger as ε grows. On the other hand, the occurrence of the frequency $q = 2$ increases as ε decreases from $\varepsilon = 0.9$ down to $\varepsilon = 0.1$, which means that the effect of the choice of α is dominant for small values of ε. This example shows very clearly the balance between α and $s(x)$ in the weakly dissipative regime. On the other side, in the same range of variation of the dissipative parameter the mapping (F) (which contains all Fourier

	(A)	(B)	(C)	(D)	(E)	(F)
$b = 0.1$	2#900	2#709	2#506	2#900	2#900	2#900
			5#297			
$b = 0.5$	2#900	2#588	2#382	2#900	2#900	2#900
		3#202	5#328			
$b = 0.9$	1#153	1#83	1#22	1#145	1#162	1#107
	2#747	2#353	2#202	2#720	2#738	2#788
		3#459	5#673	3#35		3#5
		6#3				
		9#2				

TABLE 3. Results for $\alpha = \frac{1}{2}$. The notation "$q\#n$" stands for "the periodic orbit with period q occurs n times". We limited to consider $q \leq 10$.

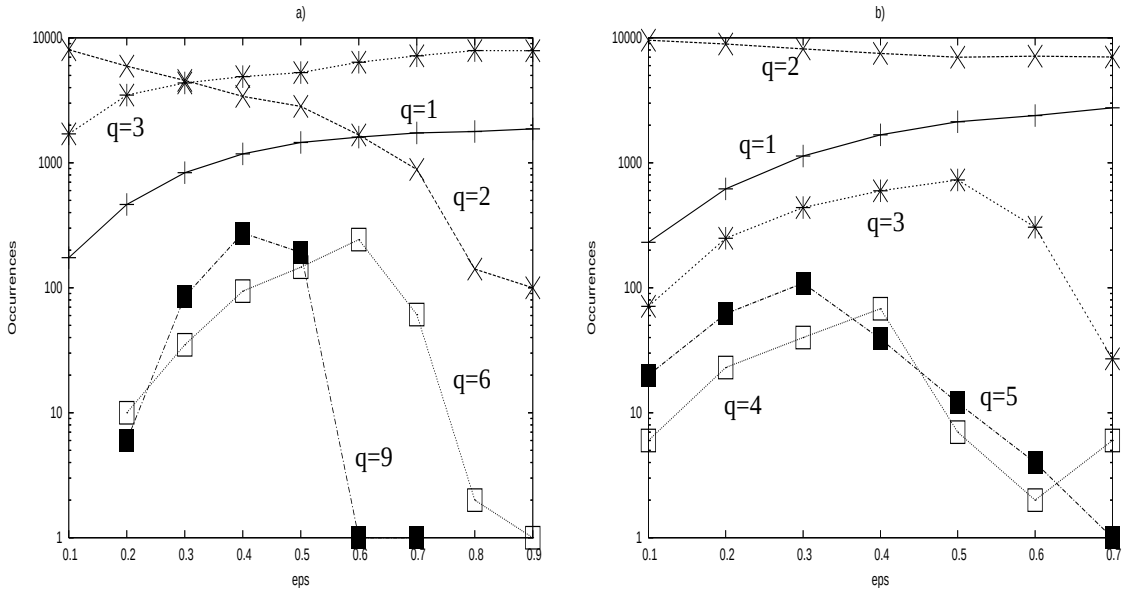

FIGURE 7. Occurrences of periodic orbit attractors versus ε: *a*) Mapping (B), $\alpha = \frac{1}{2}$. *b*) Mapping (F), $\alpha = \frac{1}{2}$.

harmonics) seems to privilege the period 2, due to the choice of the frequency α (see Figure 7*b*)). However, for increasing values of ε the number of orbits of period 2 decreases, while the number of orbits of period 1 (the main harmonic of $s(x)$) increases.

To conclude this section we investigate the transition from the weakly dissipative regime to the conservative case: let us consider the example provided by the standard mapping (A) with $\alpha = \frac{\sqrt{5}-1}{2}$ for the parameter values $\varepsilon = 0.9$ and b very close to 1. Indeed, we start by considering $b = 0.999$; after a sufficient transient number of iterations (10^7) the attractor is recognized as a periodic orbit with period 3, which

evolves into a point attractor as b is increased to 0.9999 up to $b = 0.99999$. However, taking $b = 0.999999$ the attractor is still a periodic orbit, but the period increases to 9. This attractor exists even after a larger transient time (we checked up to 10^9 iterations). The period–9 attractor is located close to the hyperbolic points of the separatrix of a periodic orbit of period 9 of the conservative case ($b = 1$) as shown in Figure 8.

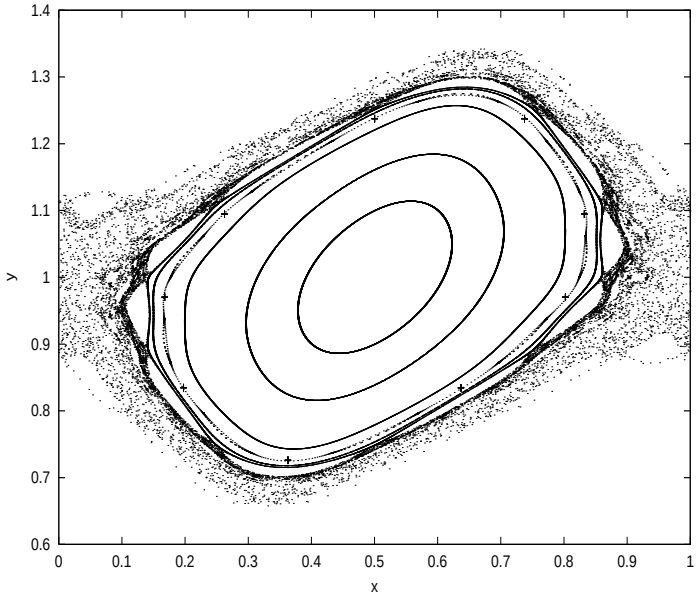

FIGURE 8. Mapping (A) with $\alpha = \frac{\sqrt{5}-1}{2}$, $\varepsilon = 0.9$. The picture shows some trajectories of the conservative case ($b = 1$) with initial conditions $y_0 = 0.9$ and $x_0 = 0$, 0.1, 0.12, 0.14, 0.15, 0.2, 0.3, 0.4 and 0.166364931496 (last value corresponds to the separatrix). Each trajectory is composed by 5000 points. The crosses provide the dynamics of the dissipative case with $b = 0.999999$ and initial conditions $y_0 = 1$, $x_0 = 0$ after a transient of 10^7 iterations.

5. **Normal form analysis.** In this section we present a normal form analysis in the framework of our nearly–integrable dissipative model problem; compare also with [5] for the investigation of perturbation properties of the fattened Arnold map and, in particular, of the existence and differentiability of invariant circles using normal hyperbolicity. We assume that the perturbing parameter is sufficiently small, so that we are allowed to expand in Taylor series around $\varepsilon = 0$; on the contrary, we do not impose any restriction on the size of the dissipative parameter (but we remark that we could exchange the roles of b and ε, by performing a normal form analysis for values of b close to 1 and for any ε). Our goal is to compute the relation between the rotation number and the original frequency of the invariant trajectory of the unperturbed system; we stress that this question does not concern the existence of a quasi–periodic attractor, which is fully investigated in [7] using a Newton algorithm.

In order to simplify the formulae which we will develop in the framework of normal form expansions, let us consider the angle variable in the interval $[0, 2\pi)$, so that instead of (2) we shall work with the following map:

$$\begin{aligned} \eta' &= b\eta + c + \varepsilon\ s(\xi) \\ \xi' &= \xi + \eta' \ , \end{aligned} \tag{11}$$

where $\eta \in \mathbf{R}$, $\xi \in [0, 2\pi)$. The link between the variables (ξ, η) in (11) and (x, y) in (2) is given by $\xi = 2\pi x$, $\eta = 2\pi y$. Moreover, let $c = (1-b)\tilde{\alpha}$, where $\tilde{\alpha} = 2\pi\alpha$. Denoting by ξ_j the j–th iterate under the mapping, from (11) we obtain $\xi_{j+1} - \xi_j = \eta_{j+1}$, $b\xi_j - b\xi_{j-1} = b\eta_j$. Casting together such relations we obtain

$$\xi_{j+1} - (1+b)\xi_j + b\xi_{j-1} \ = \ (1-b)\tilde{\alpha} + \varepsilon s(\xi_j) \ . \tag{12}$$

For ε sufficiently small, let us suppose that there exists an attractor which can be identified with an invariant curve with frequency $\tilde{\omega}$ and that such attractor is close to the invariant curve of the integrable limit (which is obtained setting $\varepsilon = 0$). Then, for a fixed value of the dissipative parameter b, we assume that the invariant curve can be parametrized by

$$\xi = \theta + u(\theta, \varepsilon) \ , \tag{13}$$

with a linear flow in the parametric coordinate, i.e. $\theta' = \theta + \tilde{\omega}$. In the following discussion we shall consider $\tilde{\omega}$ as a function of the perturbing parameter, i.e. $\tilde{\omega} = \tilde{\omega}(\varepsilon)$. Notice that such approach is different from that adopted in [7], where $\tilde{\omega}$ is fixed, while c (or equivalently α) must be varied in order to prove the existence of an invariant attractor with frequency $\tilde{\omega}$. Using $\eta_j = \xi_j - \xi_{j-1}$, one gets $\eta = \tilde{\omega}(\varepsilon) + u(\theta, \varepsilon) + u(\theta - \tilde{\omega}(\varepsilon), \varepsilon)$. Inserting (13) in (12), one obtains

$$u(\theta+\tilde{\omega}(\varepsilon), \varepsilon) - (1+b)u(\theta, \varepsilon) + bu(\theta - \tilde{\omega}(\varepsilon), \varepsilon) = -(1-b)\tilde{\omega}(\varepsilon) + (1-b)\tilde{\alpha} + \varepsilon s(\theta + u(\theta, \varepsilon)) \ . \tag{14}$$

Let us suppose that u and $\tilde{\omega}$ are analytic functions of ε around the origin, so that we can expand them in Taylor series as

$$u(\theta, \varepsilon) = \sum_{j=1}^{\infty} u_j(\theta)\varepsilon^j \ , \qquad \tilde{\omega}(\varepsilon) = \sum_{j=0}^{\infty} \tilde{\omega}_j \varepsilon^j \ . \tag{15}$$

Inserting the series expansion (15) in (14), one gets recursive relations among the coefficients $u_j(\theta)$ and $\tilde{\omega}_j$.

Let us provide the details of the explicit computation of the normal form expansion up to the order 4. By comparing the zero–order terms, it is immediate to check that $\tilde{\omega}_0 = \tilde{\alpha}$. Moreover, by (14) we obtain:

$$\begin{aligned} &\varepsilon u_1(\theta + \tilde{\alpha} + \varepsilon\tilde{\omega}_1 + \varepsilon^2\tilde{\omega}_2 + \varepsilon^3\tilde{\omega}_3) + \varepsilon^2 u_2(\theta + \tilde{\alpha} + \varepsilon\tilde{\omega}_1 + \varepsilon^2\tilde{\omega}_2) + \varepsilon^3 u_3(\theta + \tilde{\alpha} + \varepsilon\tilde{\omega}_1) + \varepsilon^4 u_4(\theta) \\ &-(1+b)\cdot(\varepsilon u_1(\theta) + \varepsilon^2 u_2(\theta) + \varepsilon^3 u_3(\theta) + \varepsilon^4 u_4(\theta)) + b(\varepsilon u_1(\theta - \tilde{\alpha} - \varepsilon\tilde{\omega}_1 - \varepsilon^2\tilde{\omega}_2 - \varepsilon^3\tilde{\omega}_3) \\ &+\varepsilon^2 u_2(\theta - \tilde{\alpha} - \varepsilon\tilde{\omega}_1 - \varepsilon^2\tilde{\omega}_2) + \varepsilon^3 u_3(\theta - \tilde{\alpha} - \varepsilon\tilde{\omega}_1) + \varepsilon^4 u_4(\theta - \tilde{\alpha})) = \\ &-(1-b)(\varepsilon\tilde{\omega}_1 + \varepsilon^2\tilde{\omega}_2 + \varepsilon^3\tilde{\omega}_3 + \varepsilon^4\tilde{\omega}_4) + \varepsilon s(\theta + \varepsilon u_1 + \varepsilon^2 u_2 + \varepsilon^3 u_3) \ . \end{aligned}$$

Comparing first order terms in ε, we get:

$$u_1(\theta + \tilde{\alpha}) - (1+b)u_1(\theta) + bu_1(\theta - \tilde{\alpha}) = -(1-b)\tilde{\omega}_1 + s(\theta) \ . \tag{16}$$

Let us expand the function u_1 in Fourier series as $u_1(\theta) = \sum_{m\in\mathbf{Z}} u_m^{(1)} e^{im\theta}$ and, to fix the ideas, let us suppose that the perturbation has the form

$$s(x) \ = \ \sin(k\xi)$$

for any $k \in \mathbf{N}$. Developing (16) in Fourier series, we get

$$\sum_{m\in\mathbf{Z}} u_m^{(1)} e^{im\theta} \cdot \left[e^{im\tilde{\alpha}} - (1+b) + be^{-im\tilde{\alpha}}\right] = -(1-b)\tilde{\omega}_1 + \frac{1}{2i}(e^{ik\theta} - e^{-ik\theta}) \ . \quad (17)$$

Once we solve (17) for $u_m^{(1)}$, we immediately recognize that the term in square brackets represents a small divisor, since it is equal to zero whenever $\tilde{\alpha}$ is a multiple of $\frac{2\pi}{m}$, i.e. $\tilde{\alpha} = 2\pi\frac{n}{m}$ for any integer n.
Moreover, for any value of $\tilde{\alpha}$ the term $e^{im\tilde{\alpha}} - (1+b) + be^{-im\tilde{\alpha}}$ is identically zero for $m = 0$, so that we must impose $\tilde{\omega}_1 = 0$. On the other side, for $m = \pm k$ we obtain $u_{\pm k}^{(1)} \cdot \left[e^{\pm ik\tilde{\alpha}} - (1+b) + be^{\mp ik\tilde{\alpha}}\right] = \frac{1}{2i}$, which determines the function u_1 as

$$u_1(\theta) = \frac{1}{2i}\Big[\frac{e^{ik\theta}}{e^{ik\tilde{\alpha}} - (1+b) + be^{-ik\tilde{\alpha}}} - \frac{e^{-ik\theta}}{e^{-ik\tilde{\alpha}} - (1+b) + be^{ik\tilde{\alpha}}}\Big] \ .$$

Notice that the function u_1 is real, since its two Fourier coefficients are complex conjugated.
In a similar way, we proceed for the second order term in ε by solving the equation for u_2 and $\tilde{\omega}_2$:

$$u_2(\theta+\tilde{\alpha}) - (1+b)u_2(\theta) + bu_2(\theta-\tilde{\alpha}) = -(1-b)\tilde{\omega}_2 + s'(\theta)u_1(\theta) \ ,$$

where $s'(\theta)$ denotes the first derivative with respect to θ (s'' and s''' will denote second and third derivatives w.r.t. θ). The average over θ of the term $s'(\theta)u_1(\theta)$ contributes to the definition of $\tilde{\omega}_2$; at present it amounts to

$$\frac{1}{2\pi}\int_0^{2\pi} s'(\theta)u_1(\theta)d\theta = \frac{1}{D_2} - \frac{1}{\bar{D}_2} \ ,$$

where $D_2 = e^{ik\tilde{\alpha}} - (1+b) + be^{-ik\tilde{\alpha}}$, while $\bar{D}_2$ is its complex conjugate. By simple computations one obtains

$$\tilde{\omega}_2 = \frac{k \ \mathrm{ctg}(\frac{\tilde{\alpha}k}{2})}{4(-1-b^2+2b\cos(\tilde{\alpha}k))} \ . \quad (18)$$

For later use, we report also the explicit expression of u_2:

$$\begin{aligned} u_2(\theta) \quad = \quad & -\frac{i}{4}\frac{ke^{2ik\theta}}{(-1-b+be^{-i\tilde{\alpha}k}+e^{i\tilde{\alpha}k})(-1-b+be^{-2i\tilde{\alpha}k}+e^{2i\tilde{\alpha}k})} \\ & +\frac{i}{4}\frac{ke^{-2ik\theta}}{(-1-b+e^{-i\tilde{\alpha}k}+be^{i\tilde{\alpha}k})(-1-b+e^{-2i\tilde{\alpha}k}+be^{2i\tilde{\alpha}k})} \ . \end{aligned}$$

From (18) we see that $\tilde{\omega}_2$ has singularities whenever $\sin(\frac{\tilde{\alpha}k}{2}) = 0$, namely $\tilde{\alpha} = 2\pi(\frac{1}{k} + \frac{\ell}{k})$ for any $\ell \in \mathbf{Z}$. Such values represent the leading zero divisors[‡] appearing in the power series representation of the rotation number $\tilde{\omega}$. We remark that the coefficient $\tilde{\omega}_2$ is zero for $\tilde{\alpha} = \pi(\frac{1}{k} + \frac{\ell}{k})$ for any $\ell \in \mathbf{Z}$.
Next, we proceed to the determination of u_3 and $\tilde{\omega}_3$ by solving the equation

$$u_3(\theta+\tilde{\alpha}) - (1+b)u_3(\theta) + bu_3(\theta-\tilde{\alpha}) = -(1-b)\tilde{\omega}_3 + s'(\theta)u_2(\theta) + \frac{1}{2}u_1^2(\theta)s''(\theta) \ .$$

[‡]Obviously, the location of the poles might change if one takes a different expression of the perturbation $s(\theta)$; however, in that case the normal form computations can be implemented through an easy generalization of the present case.

Since

$$\frac{1}{2\pi}\int_0^{2\pi}\Big[s'(\theta)u_2(\theta)+\frac{1}{2}s''(\theta)u_1^2(\theta)\Big]d\theta=0\ ,$$

we obtain that $\tilde{\omega}_3=0$. Therefore we proceed to compute u_3, which takes the following expression; let us denote by

$$A=-1-b+e^{i\tilde{\alpha}k}+be^{-i\tilde{\alpha}k}\ ,\qquad B=-1-b+e^{2i\tilde{\alpha}k}+be^{-2i\tilde{\alpha}k}\ ,\qquad C=-1-b+e^{3ik\tilde{\alpha}}+be^{-3ik\tilde{\alpha}}$$

and let the barred quantities denote the respective complex conjugates. Then, we have:

$$\begin{aligned}u_3(\theta) &= \frac{ik^2}{8}\Big[(\frac{1}{2A^3}+\frac{1}{A^2\bar{A}}-\frac{1}{A^2B})e^{ik\theta}-(\frac{1}{2\bar{A}^3}+\frac{1}{A\bar{A}^2}-\frac{1}{\bar{A}^2\bar{B}})e^{-ik\theta}\\ &\quad -(\frac{1}{2A^2C}+\frac{1}{ABC})e^{3ik\theta}+(\frac{1}{2\bar{A}^2\bar{C}}+\frac{1}{\bar{A}\bar{B}\bar{C}})e^{-3ik\theta}\Big]\end{aligned}$$

(which is immediately recognized as a real function). Finally, we proceed to compute $\tilde{\omega}_4$ as

$$\tilde{\omega}_4=\frac{1}{1-b}\cdot\frac{1}{2\pi}\int_0^{2\pi}\Big(b\tilde{\omega}_2u_2'(\theta-\tilde{\alpha})-\tilde{\omega}_2u_2'(\theta+\tilde{\alpha})+u_3(\theta)s'(\theta)+u_1(\theta)u_2(\theta)s''(\theta)+\frac{1}{6}u_1^3(\theta)s'''(\theta)\Big)d\theta\ ,$$

which can be written as

$$\tilde{\omega}_4=\frac{ik^3}{32}\Big[\frac{1}{A^3}-\frac{1}{\bar{A}^3}-\frac{3}{A\bar{A}^2}+\frac{3}{A^2\bar{A}}-\frac{2}{A^2B}+\frac{2}{\bar{A}^2\bar{B}}-\frac{2}{A\bar{A}B}+\frac{2}{A\bar{A}\bar{B}}\Big]\ .$$

New singularities appear with respect to the second order ($\tilde{\omega}_2$): beside the values $\tilde{\alpha}=2\pi(\frac{1}{k}+\frac{\ell}{k})$ for $\ell\in\mathbf{Z}$ (at which the quantity $A=0$), the function $\tilde{\omega}_4$ is singular at $\tilde{\alpha}=\pi(\frac{1}{k}+\frac{2\ell}{k})$ (at which the quantity $B=0$). It is natural to infer that the successive zero divisors will be located at the *resonances* $\tilde{\alpha}=\frac{2\pi}{n\cdot k}$; furthermore, the rate of divergence of both $\tilde{\omega}_2$ and $\tilde{\omega}_4$ increases as k gets larger or as b gets closer to 1. We recall that the overall behavior of the rotation number can be deduced from the series expansion $\tilde{\omega}=\tilde{\alpha}+\tilde{\omega}_1\varepsilon+\tilde{\omega}_2\varepsilon^2+...$

The analytical computation of $\tilde{\omega}$ as a function of $\tilde{\alpha}$ or b is in good agreement with the numerical results for any ε less or equal than 0.1 (see Figure 9). Up to this value of ε we did not remark any improvement when passing from the approximation of order 2 to that of order 4, beside the appearance of the singularity at $\tilde{\alpha}=\pi$ for the approximation of order 4 (as expected from the formula providing $\tilde{\omega}_4$). We conclude by remarking that the normal form procedure outlined before can be obviously extended to higher orders with a straightforward generalization of the previous formulae and an eventual automation through a computer implementation.

6. **Conclusions.** The analysis presented in this work represents a first step toward the study and modelling of physical phenomena described by dissipative nearly–integrable systems. Obviously, this kind of systems finds a huge variety of applications in physical frameworks; just to quote some examples, among the problems of Celestial Mechanics, we mention the non–rigid rotation of a satellite around a primary body, the Yarkovsky effect as well as the description of the evolution of a many–body system in the primordial solar nebula. The standard map–like system (2) represents the simplest dynamical model of dissipative nearly–integrable systems, though it contains all the main ingredients to provide an exhaustive description of the dynamics, populated by periodic orbit attractors, invariant curve attractors and strange attractors. In this context, we found that the final behavior

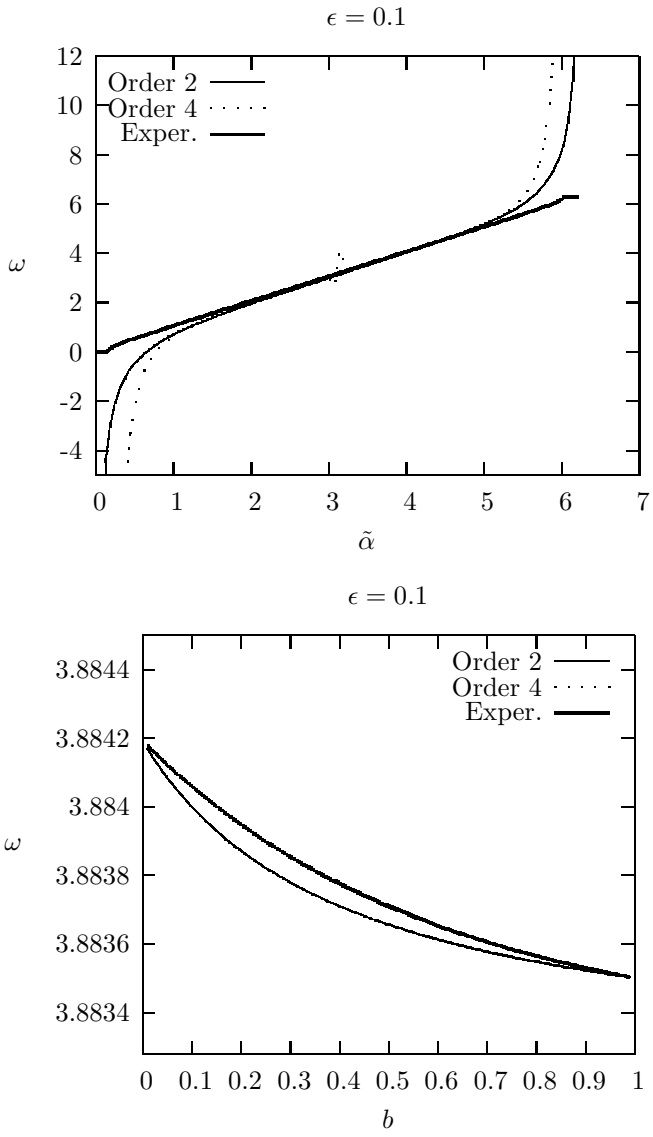

FIGURE 9. Variation of the frequency ω as a function of $\tilde{\alpha}$ (left) for $b = 0.5$ and as a function of b (right) for $\alpha = (\sqrt{5}-1)/2$. The numerical results on the mapping (A) are compared to the analytical series expansions at orders 2 and 4, which overlap in the right panel.

of the dynamics strongly depends on the choice of the frequency α as well as on the choice of the form of the mapping (i.e., the function $s(x)$ in (2)), especially when studying the weakly chaotic regime.

The investigations performed in this paper are numerical and analytical. Concerning the numerical techniques, we recall that in the last ten years a lot of tools for the global study of the dynamics of conservative systems have been developed ([22],

[20], [10], [14], [15]); their implementation allowed to obtain a deep insight on classical problems (see, e.g., [21], [28], [13], [25]). In this paper we implemented some numerical techniqus, suitably adapted to the investigation of dissipative systems. In particular, we applied two methods (which are now classical in the Hamiltonian context), namely an extension of the Fast Lyapunov Indicators (the Differential FLI) and the frequency analysis. The combined use of such techniques provides a full description of the dynamics.
Concerning the analytical investigation, we developed a normal form analysis in the framework of the nearly–integrable dissipative standard–like mapping, using Taylor series expansions (up to the order 4) in the perturbing parameter. Such normal form provides an analytical expression of the frequency of motion. A detailed study has been performed in [7] to prove analytically the existence of invariant curve attractors under smallness conditions on the parameters.

Acknowledgements. We thank G. Benettin and C. Liverani for many useful discussions and remarks. The work of A.C. was partially financially supported by COFIN/MIUR.

REFERENCES

[1] Y. Benoist, P. Foulon and F. Labourie, *Flots d'Anosov a distributions stable et instable differentiables*, J. Amer. Math. Soc., **5** (1992), 33–75.
[2] T. Bohr, P. Bak and M.H. Jensen, *Transition to chaos by interaction of resonances in dissipative systems. II. Josephson junctions, charge–density waves, and standard maps*, Phys. Rev. A **3**0, n. 4 (1984), 1970–1981.
[3] H.W. Broer, G.B. Huitema and M.B. Sevryuk, *Quasi–periodic motions in families of dynamical systems*, Springer–Verlag, LNM 1645 (1996), Berlin, Heidelberg.
[4] H.W. Broer, G.B. Huitema, F. Takens and B.L.J. Braaksma, *Unfoldings and bifurcations of quasi–periodic tori*, Memoirs Amer. Math. Soc. **8**3, n. 421 (1990), pp. vii+175.
[5] H.W. Broer, C. Simó and J.C. Tatjer, *Towards global models near homoclinic tangencies of dissipative diffeomorphisms*, Nonlinearity **1**1 (1998), 667-770.
[6] M. Casdagli, *Periodic orbits for dissipative twist maps*, Erg. Th. Dyn. Sys. **7** (1987), 165–173.
[7] A. Celletti and L. Chierchia, *Quasi–periodic solutions for dissipative standard–like maps*, Preprint (2005)
[8] A. Celletti, G. Della Penna and C. Froeschlé, *Analytical approximation of the solution of the dissipative standard map*, Int. J. Bif. Chaos **8**, n. 12 (1998), 2471–2479.
[9] B.V. Chirikov, *A Universal Instability of Many-Dimensional Oscillator Systems*, Phys. Rep. **5**2 (1979), 264–379.
[10] G. Contopoulos and N. Voglis, *A fast method for distinguishing between ordered and chaotic orbits*, Astron. Astrophys. **3**17 (1997), 73–82.
[11] M. Feigenbaum, L.P. Kadanoff and S.J. Shenker, *Quasiperiodicity in dissipative systems: a renormalization group analysis*, Physica D **5** (1982), 370–386.
[12] U. Feudel, C. Grebogi, B.R. Hunt and J.A. Yorke, *Map with more than 100 coexisting low–period periodic attractors*, Phys. Rev. E **5**4, n. 1 (1996), 71–81.
[13] C. Froeschlé, M. Guzzo and E. Lega, *Graphical evolution of the Arnold's web: from order to chaos*, Science **2**89, n. 5487 (2000), 2108–2110.
[14] C. Froeschlé and E. Lega, *On the measure of the structure around the last KAM torus before and after its break-up*, Celest. Mech. and Dynamical Astron. **6**4 (1996), 21–31.
[15] C. Froeschlé, E. Lega and R. Gonczi, *Fast Lyapunov indicators. Application to asteroidal motion*, Celest. Mech. and Dynam. Astron. **6**7 (1997), 41–62.
[16] M. Guzzo, E. Lega and C. Froeschlé, *On the numerical detection of the stability of chaotic motions in quasi–integrable systems*, Physica D **1**63 (2002), 1–25.
[17] S.Y. Kim and B. Hu, *Recurrence of invariant circles in a dissipative standardlike map*, Phys. Rev. A **4**4, n. 2 (1991), 934–939.
[18] S.Y. Kim and D.S. Lee, *Transition to chaos in a dissipative standardlike map*, Phys. Rev. A **4**5, n. 8 (1992), 5480–5487.

[19] A. N. Kolmogorov, *On the conservation of conditionally periodic motions under small perturbation of the Hamiltonian*, Dokl. Akad. Nauk. SSR **9**8 (1954), 527–530.
[20] J. Laskar, *Frequency analysis for multi-dimensional systems. Global dynamics and diffusion*, Physica D **6**7 (1993), 257–281.
[21] J. Laskar, *Large scale chaos in the solar system*, Astron. Astrophys. **2**87 (1994), L9–L12.
[22] J. Laskar, C. Froeschlé and A. Celletti, *The measure of chaos by the numerical analysis of the fundamental frequencies. Application to the standard mapping*, Physica D **5**6 (1992), 253–269.
[23] P. Le Calvez, *Existence d'orbites quasi–periodiques dans les attracteurs de Birkhoff*, Comm. Math. Ph. **1**06 (1986), 383–394.
[24] E. Lega and C. Froeschlé, *Numerical investigations of the structure around an invariant KAM torus using the frequency map analysis*, Physica D **9**5 (1996), 97–106.
[25] E. Lega, M. Guzzo and C. Froeschlé, *Detection of Arnold diffusion in Hamiltonian systems*, Physica D **1**82 (2003), 179–187.
[26] R. Lima and R.V. Mendes, *Stability of invariant circles in a class of dissipative maps*, Nonlinear Analysis, Theory, Methods and Applications **1**2, n. 10 (1988), 1061–1067.
[27] A. Neishtadt, *On averaging in two–frequency systems with small Hamiltonian and much smaller non–Hamiltonian perturbations*, Moscow Mathematical Journal **3**, n. 3 (2003), 1039–1052.
[28] D. Nesvorny and S. Ferraz-Mello, *On the asteroidal population of the first-order jovian resonances*, Icarus **1**30 (1997), 247–258.
[29] S. Ostlund, D. Rand, J. Sethna and E. Siggia, *Universal properties of the transition from quasi–periodicity to chaos in dissipative systems*, Physica D **8** (1983), 303–342.
[30] G. Schmidt and B.W. Wang, *Dissipative standard map*, Phys. Rev. A **3**2, n. 5 (1985), 2994–2999.
[31] W. Wenzel, O. Biham and C. Jayaprakash, *Periodic orbits in the dissipative standard map*, Phys. Rev. A **4**3, n. 12 (1991), 6550–6557.
[32] J. Wilbrink, *Erratic behavior of invariant circles in standard–like mappings*, Physica D **2**6 (1987), 358–368.

E-mail address: `celletti@mat.uniroma2.it; claude@obs-nice.fr; elena@obs-nice.fr`